Distribution and Statistics of African Mesoscale Convective Weather Systems Based on the ISCCP Meteosat Imagery

K. I. HODGES

Environmental Systems Science Centre and Centre for Global Atmospheric Modeling, University of Reading, Reading, United Kingdom

C. D. THORNCROFT

Department of Meteorology, University of Reading, Reading, United Kingdom

(Manuscript received 12 August 1996, in final form 18 March 1997)

ABSTRACT

This paper provides for the first time an objective short-term (8 yr) climatology of African convective weather systems based on satellite imagery. Eight years of infrared International Satellite Cloud Climatology Project–European Space Agency's Meteorological Satellite (ISCCP–Meteosat) satellite imagery has been analyzed using objective feature identification, tracking, and statistical techniques for the July, August, and September periods and the region of Africa and the adjacent Atlantic ocean. This allows various diagnostics to be computed and used to study the distribution of mesoscale and synoptic-scale convective weather systems from mesoscale cloud clusters and squall lines to tropical cyclones. An 8-yr seasonal climatology (1983–90) and the seasonal cycle of this convective activity are presented and discussed. Also discussed is the dependence of organized convection for this region, on the orography, convective, and potential instability and vertical wind shear using European Centre for Medium-Range Weather Forecasts reanalysis data.

1. Introduction

This paper presents for the first time a short-term (8 yr) climatology of summer African convective systems based on a time series of satellite imagery. Objective techniques for identification and tracking are used, and a variety of statistics are produced from the tracks, which provide information on the characteristics of the convection, for example, spatial distribution, mean propagation velocities, and genesis (where the convection is initiated). It is suggested here that to further our understanding of the tropical African climate and the interannual variability in rainfall, it is necessary to consider the climatology and interannual variability of the mesoscale convective weather systems. Such a climatology does not exist and would be of use in developing general circulation model (GCM) parameterizations of convection. This paper provides such a climatology and relates it to the large-scale atmospheric parameters as well as to geographical features.

The nature of the seasonal mean rainfall in the African Tropics and subtropics has received considerable attention during this century. This interest has been driven to a large extent by the often devastating affects of drought on people, livestock, and agriculture (e.g., Nicholson 1980). With the availability of supercomputers, efforts have been made to use GCMs to simulate and make predictions of wet and dry seasons in these regions (Rowell et al. 1995). One serious limitation of these GCM studies, however, is the coarse resolution that has to be used. A typical horizontal grid length used is 300 km, which is probably adequate for resolving synoptic easterly waves (Reed et al. 1977) but cannot represent the mesoscale convective weather systems that provide most of the rainfall in the region.

Most of the rainfall in this region is associated with either tropical squall lines (Desbois et al. 1988) or mesoscale convective complexes (Laing and Fritsch 1993), although the distinction between them is often ''fuzzy'' (Emanuel 1994). These systems, which often have horizontal scales of around 500 km, are not explicitly represented in GCM models. Limited-area models, which attempt to represent these systems (Weisman and Klemp 1982), must have grid lengths of the order of a kilometer; however, current computer power is too restrictive for GCMs to be run at this resolution. Thus, GCMs have to rely on parameterizations to account for the convection at subgrid scales.

The mesoscale convective weather systems that form over Africa during the summer months and early autumn

Corresponding author address: Dr. K. I. Hodges, ESSC (Environmental Systems Science Centre), University of Reading, Whiteknights, P.O. Box 227, Reading RG6 6AB, United Kingdom.
E-mail: admin@mail.nevc-essc.ac.uk

have been studied by several authors in the past using the Meteosat (European Space Agency's Meteorological Satellite) imagery from the International Satellite Cloud Climatology Project (ISCCP). Both objective, manual techniques (Laing and Fritsch 1993; Desbois et al. 1988) and automatic techniques (Arnaud et al. 1992) have been used. However, these previous studies have been mostly limited to a single year or a comparison between a limited number of years, due in part to the problems of handling large quantities of relatively high spatial and temporal resolution data, and the problem of identifying and tracking large numbers of ephemeral features (clouds).

A mesoscale convective weather system consists of individual convective cells and thunderstorms that are to be treated as a single entity. During the life cycle of such a system, clouds join and break away from the main complex with individual clouds or cells growing or dissipating. Thus to identify and track individual clouds and convective cells (e.g., using the techniques used to find cloud motion winds for operational forecasting) over a wide area is generally a substantial computational effort and, if manual intervention is required, both time consuming and open to subjectivity. These types of matching techniques may also have problems with missing data (images). In this study, a different approach is taken based on spatial averaging of the calibrated radiance and the identification of small numbers of representative feature points for the tracking.

Mesoscale convective weather systems have been classified according to their physical characteristics by Maddox (1980): the linear form of tropical squall lines, consisting of a line of thunderstorm cells and trailing stratiform cloud; the circular form of the mesoscale cloud cluster (MCC), identified by their extended cold cloud top or shield; and tropical storms and cyclones identified by their cyclonically curved cloud bands. There is a close relationship between MCCs and tropical storms with some eastern Atlantic tropical cyclones originating as MCCs over West Africa (Laing and Fritsch 1993). Squall lines and MCCs may also be related, with some MCCs containing or beginning as squall lines, so that ''the distinction between them is not always sharp'' (Emanuel 1994). African MCCs have lifetimes of approximately 12 h (Laing and Fritsch 1993), unless they develop into tropical cyclones over the ocean, whereas squall lines can have lifetimes that are much longer: typically 2 days (Desbois et al. 1988). In this study, no distinction is made between these forms of convective weather systems with regards to identification and tracking; the main aim is to derive a climatology of the long-lived convective weather systems rather than use current subjective classification systems, for example, that of Maddox (1980) and that used by Fritsch and coworkers.

The results presented here are for July, August, and September (JAS) and are composites of the statistics for the JAS periods of individual years in the period 1983–90. For the region of the Sahel, this period was characterized by relatively dry years compared to the long-term climatology. Included in this study will be some interpretation of the satellite-derived statistics. This will include comparison with the orography of the region, together with reanalysis data of the European Centre for Medium-Range Weather Forecasts (ECMWF) derived meteorological fields.

This study indicates that a general climatology can be constructed using smoothed satellite data that is computationally efficient, and thus long-term climatological statistics can be generated. The paper continues with a brief description of the data and its processing into gridded temperature fields, the modifications required to the tracking algorithm to deal with missing images, the presentation and discussion of the statistical diagnostic fields and their comparison with the ECMWF fields, and finally with the conclusions and further work.

2. Data processing—Tracking and statistics

The data used for this study are the ISCCP B3 reduced-resolution images (Rossow et al. 1987) derived from the *Meteosat-2, -3,* and *-4* geostationary satellites. Each image has been smoothed onto a 1.5° grid using a spherical nonparametric estimator (Hodges 1996). The tracking of the convective systems is performed using the techniques described by Hodges (1995), which have been adapted for missing data as described below. The statistical diagnostics are synthesized from the tracks using nonparametric spherical estimators (Hodges 1996) for probability densities and means.

a. Data description

The ISCCP B3 data used for this study have been derived by ISCCP from the raw full-resolution infrared (10.5–12.5 μm) Meteosat images via sampling in time and space to a temporal spacing of 3 h and a spatial resolution of approximately 30 km (Rossow et al. 1987). Each image has been normalized to a standard reference calibration and each image pixel is navigated. Thus, each pixel in the reduced images has a temperature and a latitude–longitude position associated with it.

b. Gridding of images

Maddox (1980) characterized mesoscale systems (meso α) as having length scales of 250–2500 km and timescales greater than or equal to 6 h. Thus, it is acceptable to take the ISCCP B3 satellite imagery with pixel sizes approximately 30 km and smooth the calibrated and navigated pixel values onto a rectangular 1.5° grid (approximately 150 km). At this resolution, mesoscale systems are identifiable as well as the larger synoptic-scale systems, such as tropical cyclones.

For each image the calibrated data are smoothed onto the 1.5° grid using a spherical nonparametric estimator

(Hodges 1996). This approach has been used because it is general and can be applied without the introduction of a latitudinal systematic bias. The estimate of temperature, $\hat{T}(\mathbf{X})$ at the grid point $\mathbf{X} = (x, y, z)$, where (x, y, z) are the Cartesian coordinates of the grid point with longitude and latitude (λ, θ), is given by

$$\hat{T}(\mathbf{X}) = \frac{\sum_{i=1}^{n} T(\mathbf{X}_i) K(\mathbf{X}_i, \mathbf{X}, \widetilde{C}_n)}{\sum_{i=1}^{n} K(\mathbf{X}_i, \mathbf{X}, \widetilde{C}_n)}. \quad (1)$$

Here, $T(\mathbf{X}_i)$ is the calibrated temperature for pixel i, with $\mathbf{X}_i$ the Cartesian position associated with this pixel, and n is the number of pixels. The kernel function $K(\mathbf{X}_i, \mathbf{X}, \widetilde{C}_n)$ defines the region of influence of each pixel controlled by the smoothing parameter $\widetilde{C}_n$. The summations are over all pixels, which would normally make this procedure quite time consuming, particularly if exponential kernels are used; however, by choosing relatively simple local kernel functions this can be reduced substantially. In fact, since the data point positions (pixels) are relatively constant (the error in the navigation is no more than approximately 0.2°–0.3°), this procedure can be speeded up by sorting the pixels according to whether they contribute to an estimation point, and then storing for each estimation point those pixels that do contribute. This need be done only once.

The form of the kernel used is the power kernel, specified by Hodges (1996) with an exponent of unity; thus the kernel function is given by

$$K(\mathbf{X}_i, \mathbf{X}, \widetilde{C}_n) = \begin{cases} \dfrac{\widetilde{C}_n}{\pi(\widetilde{C}_n - 1)}(\widetilde{C}_n \mathbf{X}\cdot\mathbf{X}_i - 1), & \mathbf{X}\cdot\mathbf{X}_i \geq \dfrac{1}{\widetilde{C}_n} \text{ and } \widetilde{C}_n > 1 \\ 0, & \text{otherwise.} \end{cases} \quad (2)$$

The angular bandwidth (ABW) is defined as the radial extent of the kernel function; thus, $r_b = \arccos(1/\widetilde{C}_n)$. The value chosen for $\widetilde{C}_n$ was a global value of $\widetilde{C}_n = 1.00244$, which gives an ABW of $r_b = 4°$. This value was chosen subjectively although a cross-validation value could have been determined (Hodges 1996) at some computational cost. One consequence of the gridding procedure is that the coldest gridded cloud-top temperatures (CTT) will appear warmer than the actual pixel values.

The temperature field that is generated now represents a continuous surface with a much simpler internal structure for regions that represent the convective systems, with a small number of minima representing the coldest regions of the CTT, which can be used for tracking. One drawback to this procedure is that the determination of size and shape of the mesoscale convective complexes is not now so straightforward, as the smoothing process will tend to blur the cloud edges, due to noncloudy pixel contamination, and will make the determination of size and shape dependent on the level of the thresholding. In fact for this study there is no characterization of the convective systems based on size and shape. More sophisticated techniques of identification are currently being explored that will preserve shape and areal extent, as they do not depend on the smoothing of the CTT field, and will allow these attributes to be explored with more objectivity.

c. Identification and tracking

The process of identification of the smoothed convective systems and the representative points to track begins by applying a threshold of −15°C. This is much warmer than thresholds used by previous authors due to the smoothing that has been applied. Regions are extracted as described by Hodges (1994) and minima are found for each system. The minima for each system, their positions and strengths (minimum value), are stored for each image.

The tracking is performed directly on the spherical domain as described by Hodges (1995); there is no extra cost in doing the tracking this way, and there is no latitudinal dependence in the tracking parameters. The method is essentially one of minimizing a cost function that measures the coherence in direction and speed of features (the minima in the CTT). Upper-bound constraints on the displacement distance and the track smoothness are imposed.

One problem that does occur is that of missing images. It turns out that this problem is easily solved with very little alteration to the tracking algorithm. The first step in dealing with the missing frames is to perform the tracking as if there are no missing frames using a coarse set of tracking parameters, in particular a large upper bound on the displacement distance. The ensemble of tracks are then postprocessed by performing a single forward and backward pass through the minimization algorithm (see Hodges 1994) with a more restrictive set of tracking parameters, usually a smaller upper-bound displacement. If a track is found that violates the new tracking constraints, it is checked against a database of times for the images. If the part of the track that violates the constraints coincides with missing images, the track is left unaltered; otherwise the track is broken into separate pieces. This procedure is performed on all the tracks, and on the pieces from broken tracks, until no tracks violate the constraints. There is a limit to how many consecutive missing images can be accommodated, but for the current data this is rarely more than two consecutive images.

To illustrate that the procedure outlined above can identify and track successfully the types of systems considered by previous authors, Figs. 1a–d show the four tracks from July 1983 and July 1985, which correspond

to the squall lines shown in Figs. 18a–d of Desbois et al. (1988). Notice that the tracking algorithm has successfully tracked the squall lines even though there are missing images. The second squall line (Fig 1b) has been resolved into two tracks; this is also apparent in Fig. 18b of Desbois et al. (1988). It is also apparent from the strengths of these systems that they show a diurnal cycle, as indicated by the colored points in Fig. 1. They intensify (become colder, indicating deeper convection) from early evening, while they are at their weakest during the morning. This is most clearly shown in Fig. 1a. This is in accordance with the results of Desbois et al. (1988), who measured the diurnal cycle of their detected squall lines using a volumic index (number of pixels with temperature below some threshold value). The appearance and development of convective systems during the early evening due to the formation of thunderstorms during the midafternoon has also been commented on by Laing and Fritsch (1993) for MCCs.

d. Statistics

Before computing the statistics, the tracks have been filtered according to their lifetimes at half a day (four images) so that all tracks with lifetimes of half a day and longer are retained for the statistical estimation. We are therefore only concerned with the so-called organized or long-lived convection. The statistical diagnostic fields are computed as described by Hodges (1996) using the spherical nonparametric estimators with the same kernel function specified above and using adaptive smoothing as described by Hodges (1996). The statistics that are computed are the mean strength (means of minima in the CTT), mean speed, feature density, genesis density, lysis density, track density, mean propagation velocity, and the mean lifetime. Densities are probability densities except the track density. Thus, for density $P(\mathbf{X})$, the probability of an event occurring within some small region $d\mathbf{X}$ is $P(\mathbf{X})\ d\mathbf{X}$, so that for the feature density, $P(\mathbf{X})\ d\mathbf{X}$ is the probability of finding a mesoscale cloud system within this region. For the track density this requires normalization (Hodges 1996). The missing images are taken account of for those statistics where it is important, for example, mean propagation velocities, mean speeds, mean lifetimes, genesis, and lysis. Such statistics have been estimated before (e.g., Laing and Fritsch 1993; Desbois et al. 1988), but this is the first attempt at producing a mean view calculated over many years. Before considering the storm statistics, the important thermodynamic and dynamic fields that influence the nature of the long-lived convective systems are first examined.

3. ECMWF reanalyses and orography

a. Background

The mesoscale convective weather systems observed over tropical Africa are generally considered to be triggered (e.g., Hastenrath 1991), for example, in association with orography and elevated daytime heating (e.g., Rowell and Milford 1993) or synoptic weather systems such as easterly waves (e.g., Machado et al. 1993). According to Emanuel (1994) this ''type I'' convection relies on the buildup of large amounts of convective available potential energy (CAPE). In the tropical north African region, such a buildup arises in association with surface fluxes and through the low-level advection of cool moist high-θ_e air from the Gulf of Guinea below the much drier and hotter high-θ_e air originating from the northern Saharan region. Together with the large vertical wind shear below about 600 mb associated with the African easterly jet (AEJ), the tropical north African region and in particular the western African region is well known to be associated with an environment conducive for organized long-lived convection (e.g., Chong et al. 1987). For comparison with the the satellite-derived storm statistics in section 4, the orography of the tropical north African region together with mean θ_e and wind fields are presented here. The meteorological fields are derived from the T106 ECMWF reanalysis uninitialized dataset and averaged between 1983 and 1990, for July–September. However, it should be realized that the ECMWF reanalyses are subject to errors, in association with lack of observations and the limitations of model parameterizations, and should not be viewed as truth. Despite this, they probably represent the best coherent four-dimensional dataset of large-scale atmospheric properties that can be used for comparison with satellite-derived diagnostics.

b. Orography

Figure 2 shows those regions of tropical Africa where the land has an elevation greater than 500 m. The elevated terrain at latitudes within the main summer rain belt north of the equator include, going from east to west, the Ethiopian highlands, Dhafur, Cameroon highlands, Jos, and the Guinea highlands. After the Ethiopian highlands, the next highest region of tropical Africa are the highlands surrounding Lake Victoria near the equator. Although attention in the past has mostly been given to the region north of this, it will be shown here that the northern summer deep convection also occurs over a wide region west of these mountains. This region in the Congo basin is characterized by moist marshy lowlands that provide moisture for convection. The mountains north of 15°N including Tibesti, Aïr, and the Hoggar are all north of the main summer rain belt and, from this study, do not appear to be important for triggering long-lived convection.

c. Equivalent potential temperature (θ_e) and saturated equivalent potential temperature (θ_{es})

1) ZONALLY AVERAGED SECTION

Figure 3a shows a vertical cross section of the JAS mean θ_e averaged between 15°W and 30°E, and averaged

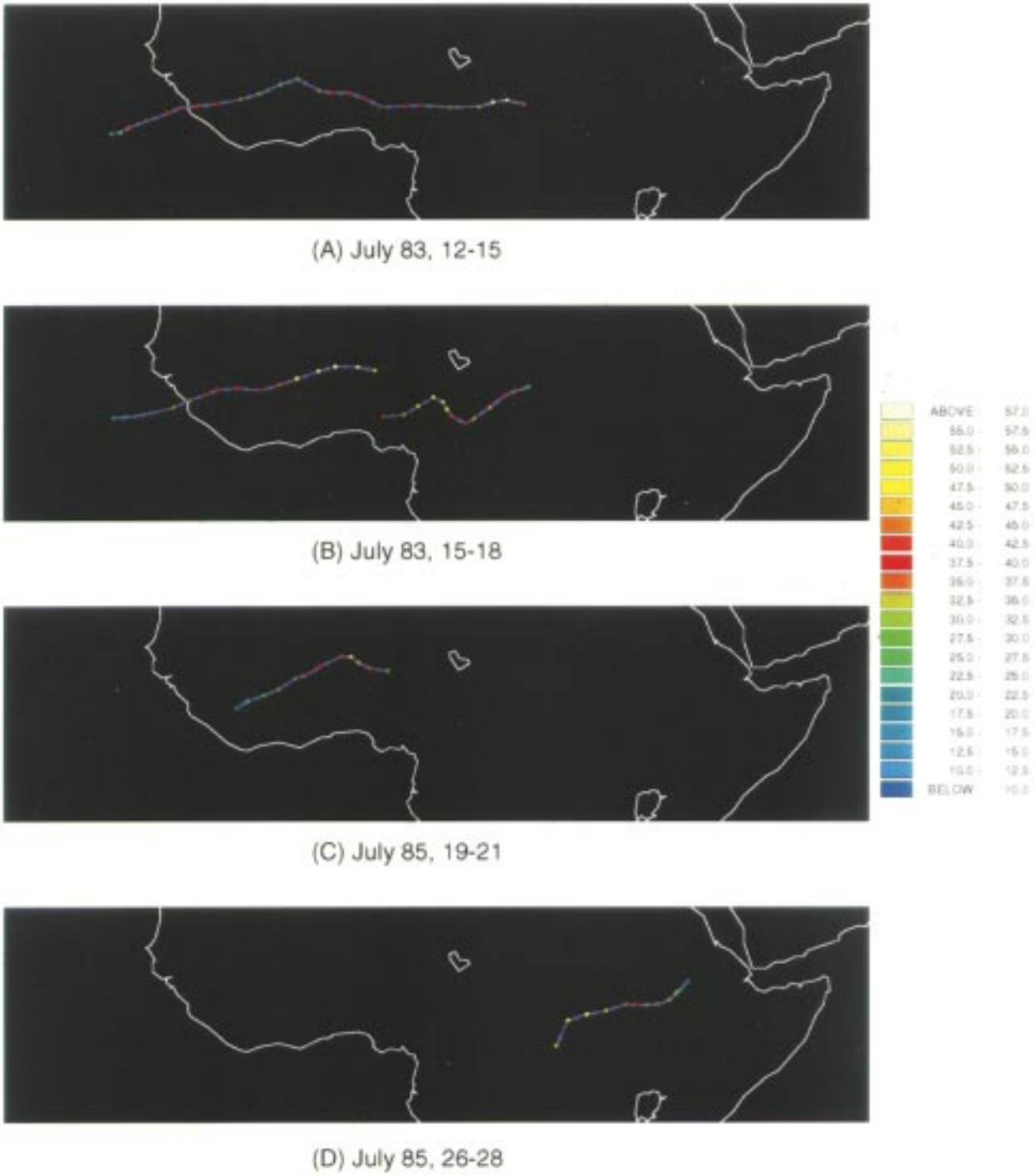

FIG. 1. Tracks of the squall lines obtained by the tracking code that correspond to those obtained by Desbois et al. (1988) for 1983 and 1985; (a) 12–15 July 1983, starting time 1800 (12 July), finish time 1800 (15 July), missing image at 0900 (13 July); (b) 15–18 July 1983, starting time 0600 (15 July), finish time 1800 (18 July), separation 1800 (16 July), missing image 0900 (18 July); (c) 19–21 July 1985, starting time 1800 (19 July), finish time 0000 (21 July); (d) 26–28 July 1985, starting time 1500 (26 July), finish time 0000 (28 July). Temperatures are relative to 0°C.

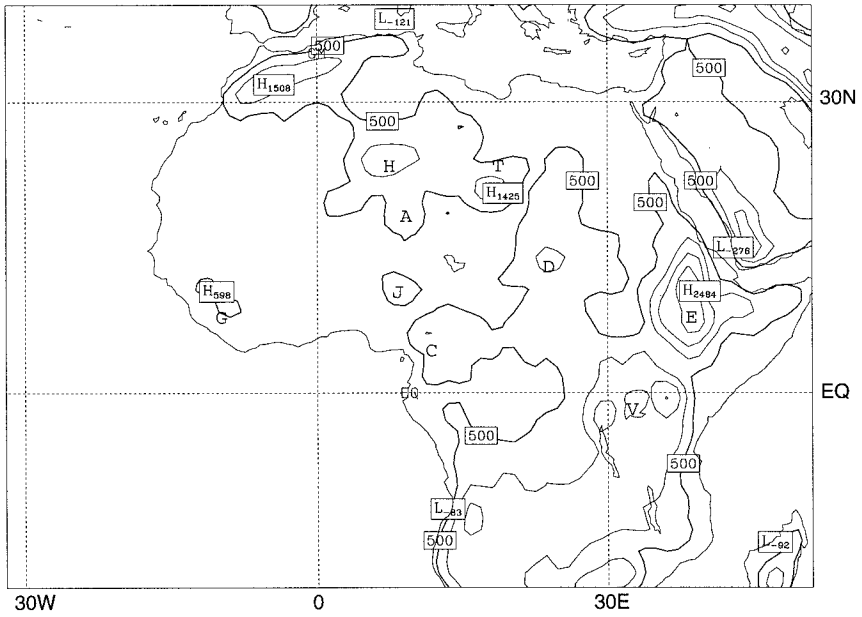

FIG. 2. The general orography of the tropical African region taken from the ECMWF reanalyses (contour interval 500 m). Regions discussed in the text are indicated by the bold characters, going from east to west. E: Ethiopian highlands; V: Lake Victoria; D: Darfur; T: Tibesti; C: Cameroon highlands (Massif de L' Adamaoua, Gotel Mountains, Shebshi Mountains); J: Jos; A: Aïr; H: Hoggar; G: Guinea highlands.

in time between 1983 and 1990. The region between about 2° and 15°N is characterized by a maximum in θ_e at low levels in association with a potentially unstable mean thermodynamic profile. Note also the strong vertical gradient in θ_e near the surface (seen more strongly in θ_{es}, Fig. 3b); this is associated with nighttime cooling at the surface. Figure 3b shows a vertical cross section of the JAS mean θ_{es}, averaged between 15°W and 30°E, and averaged in time between 1983 and 1990. Now since θ_{es} is a function of pressure and temperature only, the maximum is found north of the θ_e maximum at low levels in the hot desert region. The negative vertical θ_{es} gradient there implies strong conditional instability; however, since in this region the humidity is very small (cf. with low θ_e values in Fig. 3a), this instability is unlikely to be realized. This fact can be illustrated by considering the height at which low-level air, if lifted, will become buoyant. Heights at several latitudes at which low-level air when lifted becomes buoyant have been estimated using Figs. 3a,b. The dashed line in Fig. 3a represents the level of free convection (LFC) based on these estimates. The high LFC in the Saharan region clearly illustrates that although the low-level air is conditionally unstable, this instability is unlikely to be realized. The low LFC equatorward of this occurs in the region of high low-level θ_e and also in latitudes much more related to observed rainfall and storm activity. Thermodynamic patterns of instability are therefore much more usefully diagnosed using θ_e and its vertical gradient than by using θ_{es}. Note that this does not mean that all convection over tropical north Africa occurs through the release of potential instability (PI). It is simply that θ_{es} is not a useful diagnostic quantity for determining regions of realizable thermodynamic instability over North Africa due to its dependence on just temperature and pressure.

The fact that potentially and conditionally unstable air is present in this time mean is consistent with the idea presented by Emanuel (1994) for triggered convection whereby CAPE is released on a timescale longer than that for it to build up. This results in the often very vigorous storms seen over continental tropical Africa in summer associated with the sudden release of large CAPE. It is clear therefore that on individual days the thermodynamic profiles will exhibit greater instability than seen here because the mean comprises days exhibiting instability as well as stability; the latter is expected after convection has acted to stabilize the profile. In order to see the geographical distribution of the thermodynamic instability of the tropical African region, two measures of mean unstable profiles will be shown below: Fig. 4a, the surface θ_e, and Fig. 4b, the difference between θ_e at the sigma model levels of $\sigma = 1.0$ and $\sigma = 0.65$.

2) HORIZONTAL SECTIONS

Figure 4a shows the mean surface θ_e distribution for the tropical African region. As discussed by Thorncroft and Haile (1995), for July 1989 there is a general NW–SE tilt of the maximum low-level θ_e values across Africa associated with the low-level meridional wind distribution, with moist southerlies penetrating poleward in the west and dry northerlies penetrating equatorward in the east. There are also high values in the Congo region

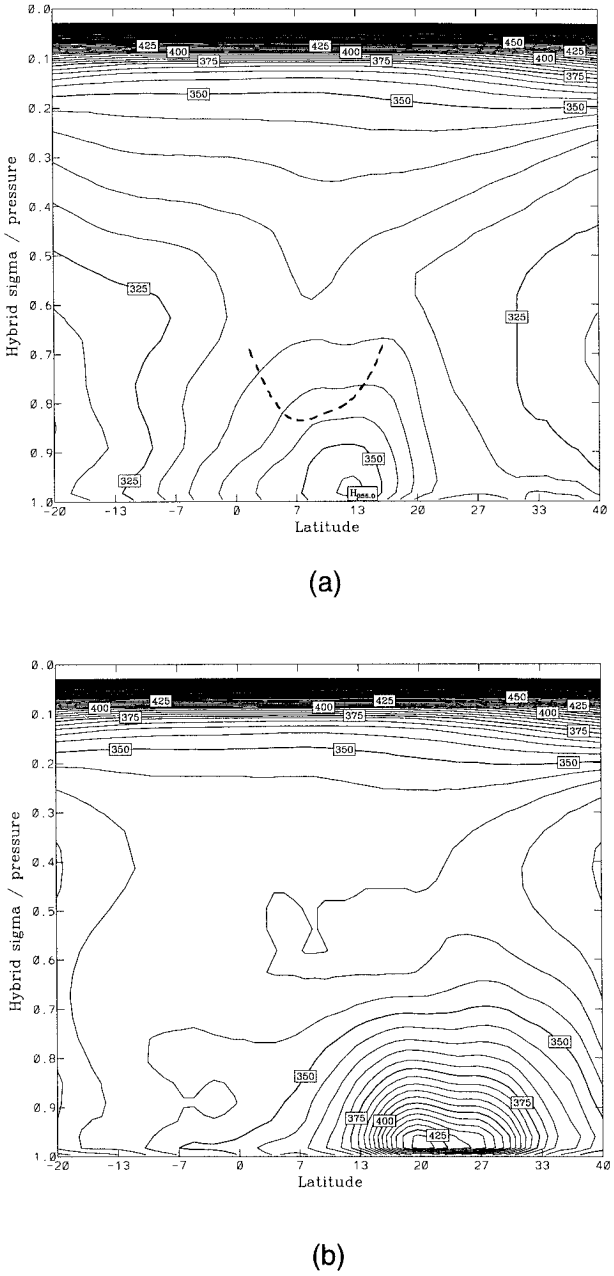

FIG. 3. (a) Vertical cross section of θ_e averaged between 15°W and 30°E and JAS 1983–90 (contour interval 5 K). (b) Vertical cross section of θ_{es} averaged between 15°W and 30°E and JAS 1983–90 (contour interval 5 K), for tropical Africa. These have been computed from the ECMWF reanalyses.

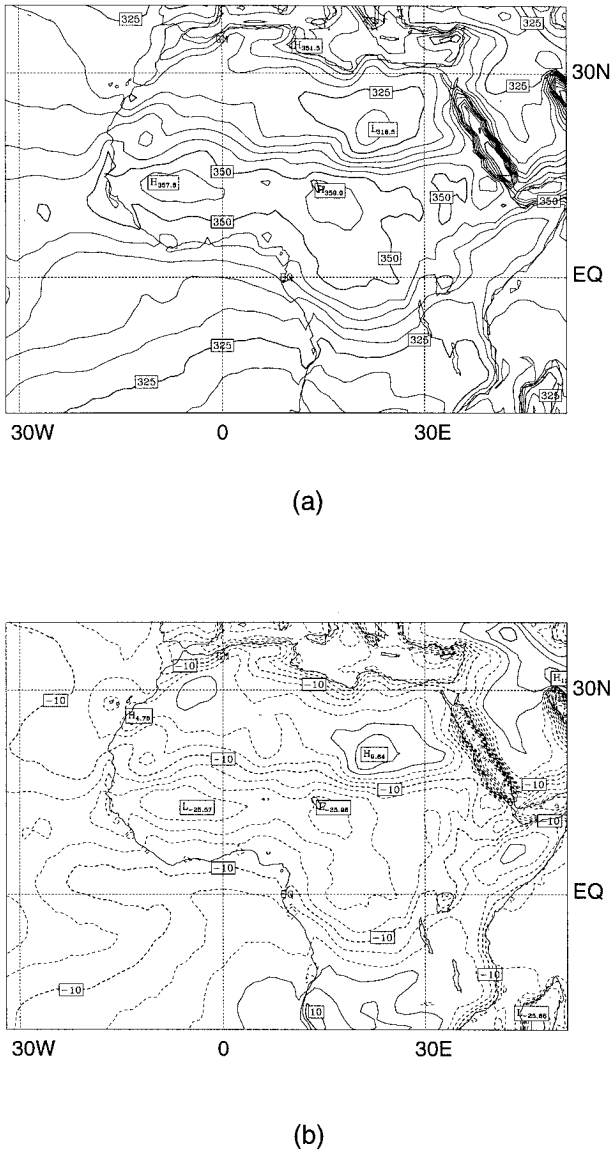

FIG. 4. (a) Contour map of tropical African θ_e averaged over JAS 1983–90 (contour interval 5 K). (b) Contour map of tropical African PI averaged over JAS 1983–90 (contour interval 4 K), computed from the ECMWF reanalyses.

in association with the moist lowlands and southwesterly flow from the tropical Atlantic. These high-θ_e regions are also associated with PI (see below) and indicate preferred regions of convection. This is confirmed below by considering the mean outgoing longwave radiation (OLR) of the region.

In Fig. 4a note how the low-level θ_e decreases rapidly between the west coast and the ocean. Low-level northerlies on the eastern flank of the Atlantic anticyclone result in upwelling waters and cold SSTs. As well as lower θ_e values, at low levels the potential and conditional instability is markedly less too. This would suggest that mesoscale convective weather systems tracking over the ocean will have to adjust to a markedly different environment and may actually decay. These cold SSTs may also influence those weather systems tracking far enough westward to initiate tropical cyclones; for example, 1994 was associated with anomalously cold waters in this region west of the Guinea highlands and also with an anomalously weak tropical cyclone season.

The contours included in Fig. 4b are a measure of

the PI. These represent the difference between θ_e at the sigma levels of $\sigma = 1.0$ and $\sigma = 0.63$, where negative values indicate possible instability. The sigma-level data has been used here in order to provide sensible values over the orography (cf. Fig. 2). Comparing the PI pattern with the low-level θ_e shows that high values of low-level θ_e are generally well correlated with high PI. This is also consistent with the work of Williams and Renno (1993), who showed a good correlation with low-level θ_w and CAPE. It is of interest to note the large contrasts between the land and ocean, with PI large over the land and much smaller over the ocean. Thus, it appears that the statistical equilibrium ideas of Emanuel (1994) clearly appear less relevant to continental Africa than to the tropical oceans. Also note, however, the fairly rapid transition from high PI to much lower PI, going from the land to the ocean. This suggests that the zonal advection of temperature and humidity from Africa to the ocean are much less important than the local surface fluxes in influencing the convective equilibrium.

d. Zonal wind

1) ZONALLY AVERAGED SECTION

Figure 5 shows a vertical cross section of the JAS mean zonal wind averaged between 15°W and 30°E and averaged in time between 1983 and 1990. The zonal wind is important for two reasons: (a) it steers the storms and therefore influences the rainfall distribution, and (b) as discussed by Weisman and Klemp (1982), it acts to organize the convection so that it can be long lived. Note the presence of the midtropospheric easterly jet around 600 mb. The mean value seen here of around 10 m s^{-1} is expected to be lower than that that would be seen on an individual day due to the smoothing associated with the seasonal and yearly averaging. As noted by Thorncroft and Haile (1995), the strongest vertical shear exists at the same latitudes as the regions of high low-level θ_e and PI. This may be understood by considering the fact that the strong shear is associated with the strong horizontal temperature gradient that exists between the Sahara and the Guinea coast. Since at low levels the hottest air is to the north of the region and the moistest air is to the south of the region, θ_e, which is a function of both, is a maximum between the two, that is, at the jet latitude. Figure 5 clearly indicates the presence of marked wind shear between about 600 mb and low levels, which is known to be conducive for organized convection. The geographical distribution of this shear is indicated below.

2) HORIZONTAL SECTIONS

Figure 6 shows the mean wind shear between $\sigma = 1.0$ and $\sigma = 0.63$ (as before, sigma-level data is used to provide sensible values over the orography). The strongest shear occurs in the tropical west African region in association with the region of strongest low-level temperature gradient (not shown) and the AEJ. East of about 10°E the shear vector weakens consistent with a weakening jet. Also indicated in Fig. 6 is a region of much weaker vertical shear situated in the equatorial Congo region. Since long-lived convection is associated with strong vertical shear and high low-level θ_e, Fig. 6 suggests that the preferred region is in tropical west Africa around 10°N. The Congo basin region between 10° and 20°E is a region with high low-level θ_e but weaker vertical shear, so that convection is to be expected but may be less well organized than in the tropical west African region.

e. Summary

The ECMWF reanalysis fields presented here indicate that there are large regions in the tropical African region where the atmosphere is able to support strong moist convection, coexisting with regions of significant vertical wind shear. Indeed, as was noted by Thorncroft and Haile (1995), it seems that high low-level θ_e is generally positively correlated with strong vertical wind shear. Together with the significant orographical features providing the necessary triggers, as well as easterly waves, the region is expected to be associated with organized long-lived convective weather systems, as has been shown previously. The results from the analysis of the satellite data will now be examined and compared with these mean fields.

4. Eight-year average storm activity

a. Mean outgoing longwave radiation

For comparison with the statistics examined below, the mean outgoing longwave radiation (OLR) for the period of this study is shown in Fig. 7. The main convection regions that can be seen occur in similar regions to those discussed in Desbois et al. (1988), with notable maxima associated with elevated terrain (cf. Fig. 2). A broad region of high mean cloud is present between about 18°N and the equator with enhanced regions over the Ethiopian highlands, the Cameroon highlands, and the Guinea highlands. Other important regions include the Sahelian zone around 15°N and the zone west and north of Lake Victoria in the Congo basin. Note also the equatorward shift of the main convection region moving from the African continent to the tropical ocean. The OLR distribution has considerable similarities to the mean low-level θ_e and PI pattern, which gives some confidence in the ECMWF analyses. The next sections examine the nature of the convecting systems that contribute to the mean picture of Fig. 7.

b. Eight-year statistics for July, August, September 1983–1990

The results for the 8 yr of JAS periods are shown in Fig. 8.

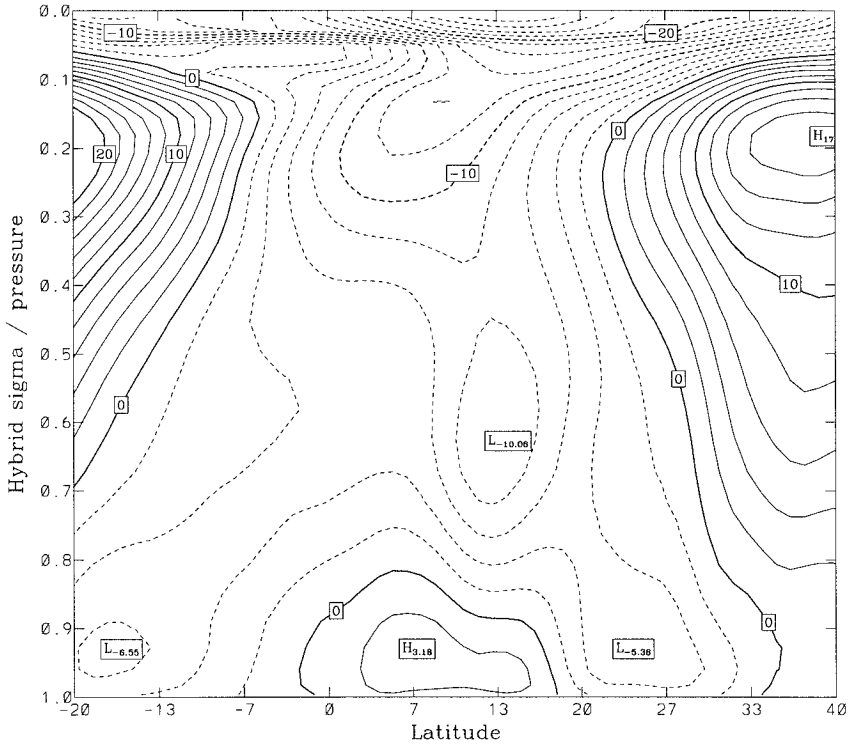

FIG. 5. Vertical cross section of the mean zonal wind averaged over JAS 1983–90 between 15°W and 30°E (contour interval 2 m s^{-1}), computed from the ECMWF reanalyses.

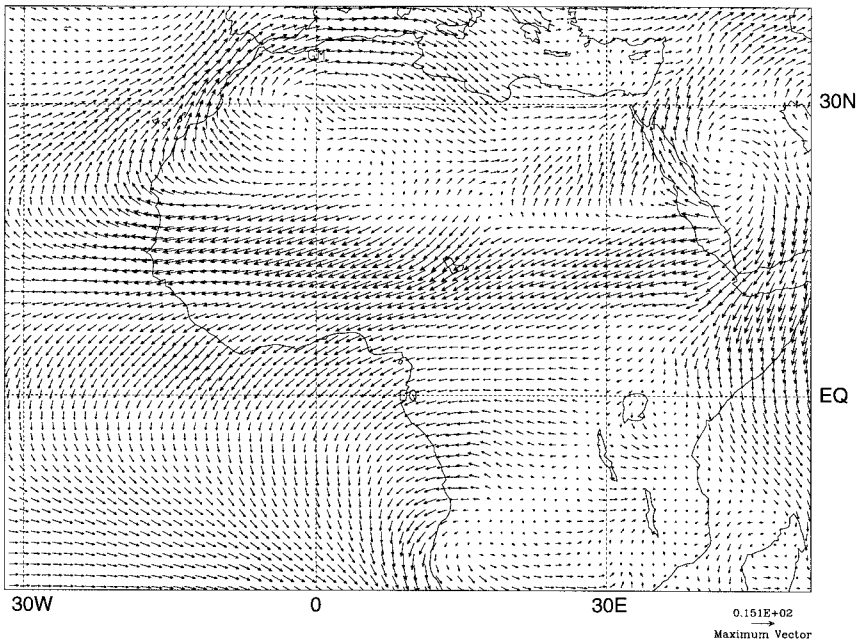

FIG. 6. Mean wind shear vectors computed between $\sigma = 1.0$ and $\sigma = 0.63$ and averaged over JAS 1983–90, computed from the ECMWF reanalyses.

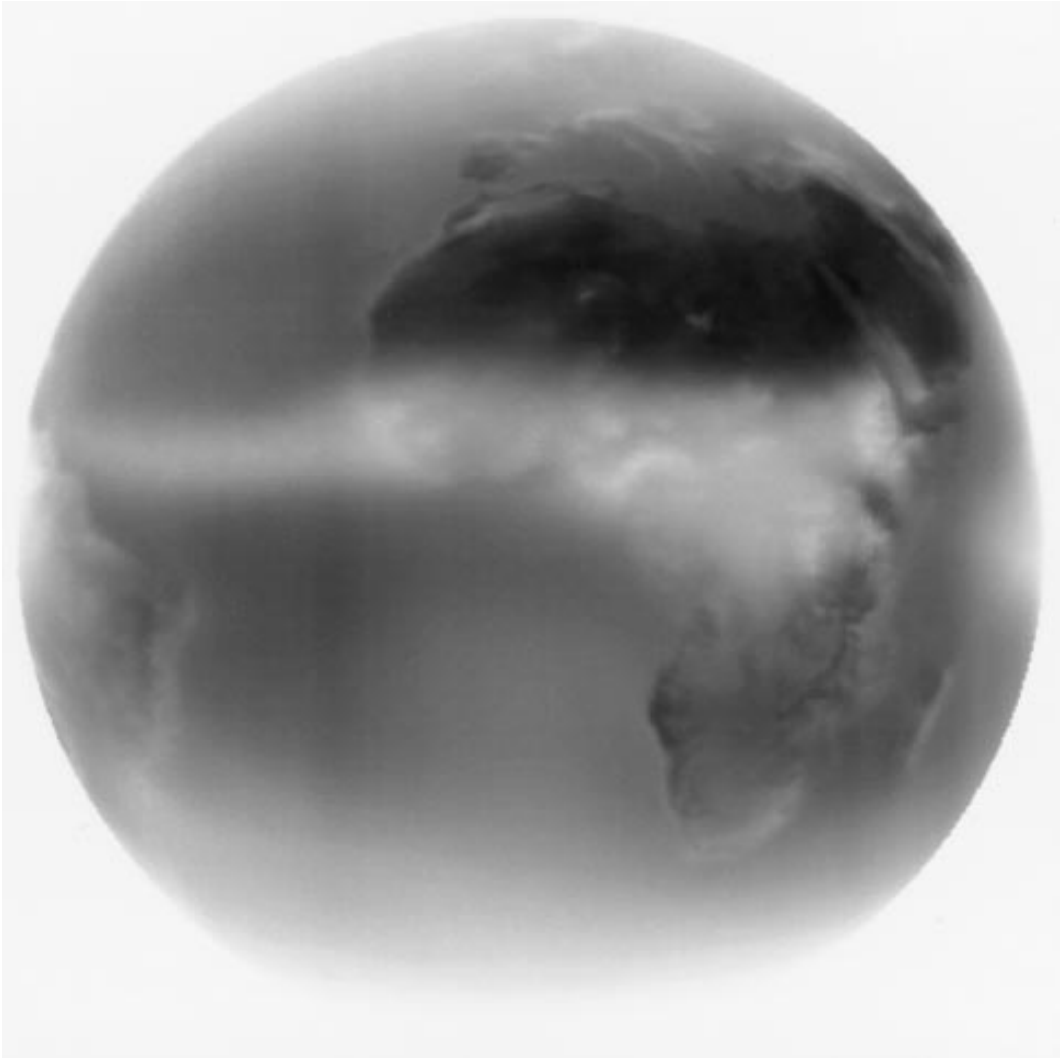

FIG. 7. The 8-yr JAS mean OLR, contrast enhanced image.

1) FEATURE DENSITY

The feature density shown in Fig. 8c bears considerable similarities to the mean OLR shown in Fig. 7. This would have been expected since the regions of greatest convective cloud cover in the mean OLR are composed of the types of features that contribute to the feature density, that is, convective cloud complexes. The northern limit of the feature density also slopes equatorward west of the coast and can be associated with the marked mean northerly wind present on the eastern flank of the Atlantic high and, as mentioned earlier, the cold SSTs there.

Within the main activity, several maxima exist: over the Ethiopian highlands, the Jos and Cameroon highlands, and the Guinea highlands near the west coast. Weaker maxima exist over the southern edge of the Dhafur mountains, the Adamaoua highlands, and southeast from Dhafur. It is noticeable that a significant region of high feature density extends westward across the Atlantic. It is likely that some of the weather systems identified here are associated with the triggering of tropical cyclones (Avila and Pasch 1992). It would be interesting to relate, in future work, the interannual variability of the feature density on the Guinea coast with the interannual variability of tropical cyclones since it has already been shown that the Sahelian seasonal rainfall anomaly has strong links to tropical cyclone activity in the Atlantic (Landsea and Gray 1992).

2) GENESIS DENSITY

The genesis density shown in Fig. 8d has five notable maxima over land. These are the Ethiopian highlands, northwest of Lake Victoria, south of Dhafur, the Cameroon and Jos region, and the Guinea highlands. Notable regions of low genesis are in the region between Dhafur

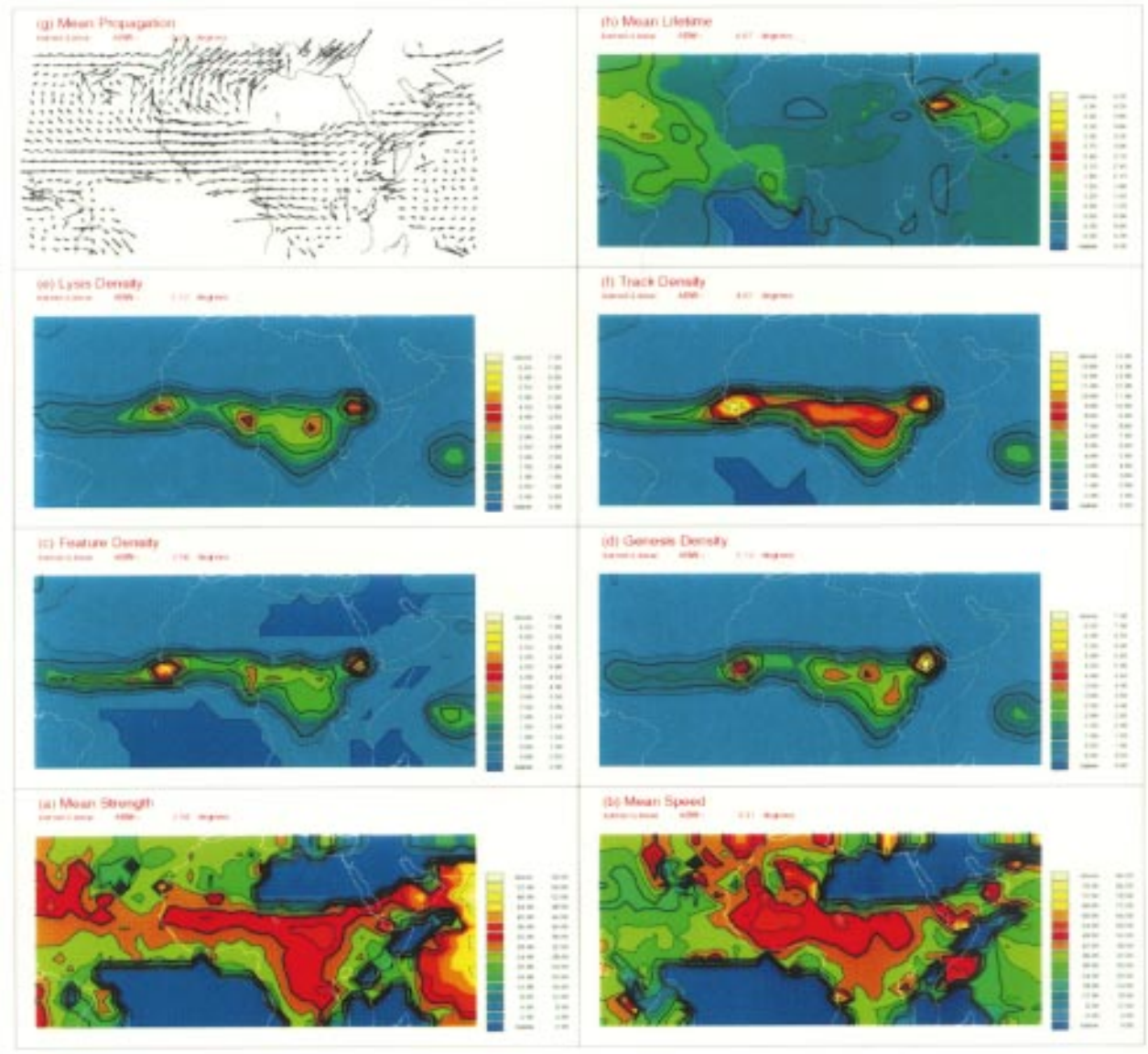

FIG. 8. The July, August, and September composite statistics for the 8-yr period 1983–90: (a) mean strength (degrees Celsius below 0°C), (b) mean speed (km h^{-1}), (c) feature density, (d) genesis density, (e) lysis density, (f) track density, (g) mean propagation, and (h) mean lifetime (days).

and the Ethiopian highlands and also between the Cameroon and Guinea highlands. As seen in Fig. 2, these are regions of low elevation. Low genesis is found north of the Guinea coast in the Sahelian zone and also over the ocean west of the African coast. Clearly, the orography is the main trigger of mesoscale convection in the tropical African region in agreement with Rowell and Milford (1993).

3) MEAN SPEED AND PROPAGATION

The mean propagation velocity of storms shown in Fig. 8g shows that storms generally move westward. Notable exceptions include the storms initiated over the Ethiopian highlands, which predominately move southwestward. This is probably due to the unfavorable meteorological conditions for organized convection immediately west of the Ethiopian highlands (cf. Figs. 4a and 6). The low-level θ_e, as well as vertical wind shear, are low compared with other areas in the vicinity. By considering the potential instability, shown in Fig. 4b, it appears that the storms have a track that follows the maximum PI. Mean speeds (Fig. 8b) in the convectively active region described above are approximately 40–60 km h^{-1} (10–17 m s^{-1}), with the maximum speeds attained around Lake Chad and the region of Burkina-

Faso, Mali, and Niger, which is roughly consistent with where the AEJ is strongest (cf. Fig. 6). To the west of the west African coast, speeds reduce to approximately 25–40 km h^{-1} (7–10 m s^{-1}). The northward propagating systems giving rise to the propagation vectors seen in the northwest of Africa are due to isolated precipitation systems (cf. low feature density) generated in the autumn (September in this case) in the monsoon trough; these are generally weak systems (cf. mean strength). The lower values of the mean strength (warmer CTT indicate that these are likely to be low-level precipitation systems and not high-level cirrus. The indication of systems entering the main band of activity from the east over Saudi Arabia is again due to isolated systems (cf. feature density) generated in the Arabian Sea and Persian Gulf; these can be quite intense convectively active systems (cf. mean strength, cold CTT). In summary, for the high convective activity regions, storms track predominately westward except those storms west of the Ethiopian highlands. The storms in the Congo basin are also strong but move more slowly, consistent with weaker winds and shear (cf. Fig. 6)

4) MEAN LIFETIME

This statistic is for storms passing through a region. The main points to observe in Fig. 8h are that the Ethiopian highlands are characterized by short-lived storms (approximately 0.5–1.0 days) and that the longer-lived storms are initiated farther west in the Sahel, since the direction of propagation is predominately westward, as discussed previously. Over the ocean lifetimes are approximately 2 days, although this will be biased at the western limit of the region as systems move out of the field of view. In the Congo, convective systems are short lived and do not reach the coast.

5) MEAN STRENGTH

The mean strength of systems shown in Fig. 8a indicates where regions of deep convective activity occur in terms of the CTT measured relative to 0°C; the colder the CTT, the deeper the convection. From this figure there is a clear tendency for the strongest storms to occur in the northern part of the feature density pattern around 15°N as well as north and west of Lake Victoria. The storms tend to be weaker just west of the mainland but strengthen again downstream. As mentioned above, the isolated storms over northwest Africa are relatively weak, while those coming from Saudi Arabia can be quite intense. The narrow region of strong storms in the Sahelian region are in the vicinity of the strongest wind shear and high low-level θ_e. This is obviously a region conducive to long-lived organized severe convection. Similarly, the region west of Lake Victoria is also a region of weaker shear but strong PI and so the convective complexes are less long lived as they do not have such a favorable environment.

6) LYSIS DENSITY

The lysis density pattern (Fig. 8e), like the genesis pattern, appears to be determined by the orography. This is because many of the storms are short lived and therefore do not move far from the region in which they are initiated. Notice the slight shift of the maxima in the lysis density westward from the same maxima in the genesis, which is particularly noticeable over the Guinea highlands. It is also suggested here that downstream orography can inhibit propagation of storms initiated upstream (cf. section 4c). The lysis over the ocean is likely to be associated with the cold SST leading to a reduced magnitude of PI (cf. Fig. 4b). The predominance of short-lived storms over the orography may be due to the fact that there is usually significant CAPE for convection but not always sufficient shear for organization. More detailed analysis of the intraseasonal variabilty of CAPE and shear is needed to confirm this point.

c. Further analysis of genesis and lysis

To analyze these results further, the systems that contribute to the regions of genesis and lysis discussed above have been binned according to their lifetimes, initiation (genesis) times, dissipation (lysis) times, and displacement distances. For each of these binned quantities, the frequencies are calculated. The regions considered are shown in Fig. 9. The frequencies are shown in Figs. 10 and 11.

1) GENESIS REGIONS 1 AND 2

Both of these regions are characterized by high PI and low vertical shear. The storms initiated in these regions are predominately short lived (approximately 12–18 h) and have small displacement distances, with the mode of displacement at about 400 km. A few storms traveled up to 2500 km, which implies that storms originating in the Ethiopian highlands do not travel farther west than about 15°E; this would suggest lysis in the region of the Cameroon highlands. There is a perceptible shift to slightly longer lifetimes and displacement distances in region 2. The initiation times for mesoscale convective systems in regions 1 and 2 are strongly peaked at 1500 UTC (1700 LT) in both cases. Thus, convective systems in these regions show a strong diurnal character with the majority remaining within the region or close proximity.

2) GENESIS REGIONS 4, 5, AND 7

These are regions where much longer-lived storms are generated. Again, there is a strong diurnal cycle in the initiation times, but storms can be initiated at any time. There is a shift to slightly later preferred initiation times the farther west the region is, with region 7 show-

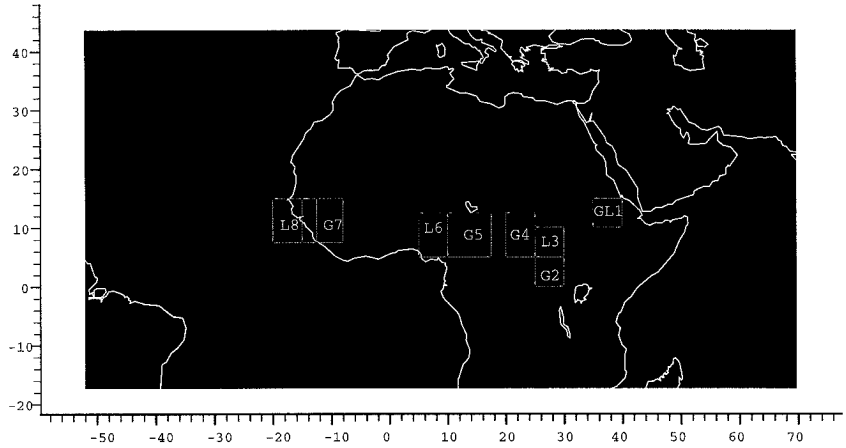

FIG. 9. Analysis regions for binning; G represents a genesis region and L is a lysis region. The numbers are identifiers.

ing a preferred time peak at 1800 UTC (1800 LT). This shift to later initiation times is due to the solar heating occurring later in the UTC day in the west (initiation times are similar according to local time). The distribution of the lifetimes is seen to broaden with many more longer-lived systems generated in these regions than in the previously discussed regions. This is also reflected in the displacement distances, which show the main mode displaced toward longer distances around 800 km and with many more systems traveling as far 2000 km. This is a result of longer-lived systems and also of larger propagation velocities within and to the west of these regions. It is likely that many of these weather systems are squall lines as observed by Desbois et al (1988).

3) LYSIS REGIONS 1 AND 3

These two regions are similar and are characterized by short-lived, small displacement storms (approximately 400 km) consistent with regions 1 and 2 discussed above. The preferred dissipation times are in the early morning at 0300–0600 UTC (0500–0800 LT), although storms dissipate throughout the day.

4) LYSIS REGION 6

Many storms that dissipate in this region have traveled much farther than those in regions 1 and 3, probably from regions 4 and 5. Thus, it appears that storms that dissipate here are a mixture of short-lived storms initiated locally and longer-lived storms initiated remotely with lifetimes as long as 40 h and displacement distances as much as 3000 km. Dissipation times are now predominately at 0600 UTC (0700 LT), and are associated with the short-lived storms but with dissipation at other times as well, probably associated with longer-lived storms.

5) LYSIS REGION 8

This region is similar to region 6 but has a much broader distribution of dissipation times, probably due to a broad range of storms initiated remotely. There is a marked minima in the dissipation times at 1200 UTC (1200 LT), which was also perceptible in region 6. It is suggested that this is the time when CAPE and surface θ_e are expected to be largest; so when CAPE is strong, unless there is a strong dynamical influence associated with an easterly wave, for example, we do not expect lysis.

d. Seasonal cycle

For completeness the monthly composite statistics of feature density, genesis density, and lysis density for July, August, and September are presented, in Fig. 12, to illustrate the mean observed seasonal cycle. It is well known (e.g., Hastenrath 1991) that the tropical African region is characterized by a rainfall maximum that moves poleward during July and August and retreats equatorward in September. The storm statistics presented in Fig. 12 are mostly consistent with this. For example, although the feature density for each month, shown in Fig. 12, has a very similar pattern to the JAS distribution shown in Fig. 8, the amplitudes change during the season. In particular, the maxima associated with the Ethiopean highlands, the region equatorward and downstream of Dhafur, and the Guinea highland coastal region are greater in July and August than in September. In contrast the maxima associated with the Cameroon, Jos, and Congo regions are more pronounced in September and weakest in August, which is again consistent with known seasonal meridional shifts in maximum rainfall.

The most unexpected result, however, is in relation to the Guinea highland coastal region maximum, which in July is shifted over the ocean west of its location in

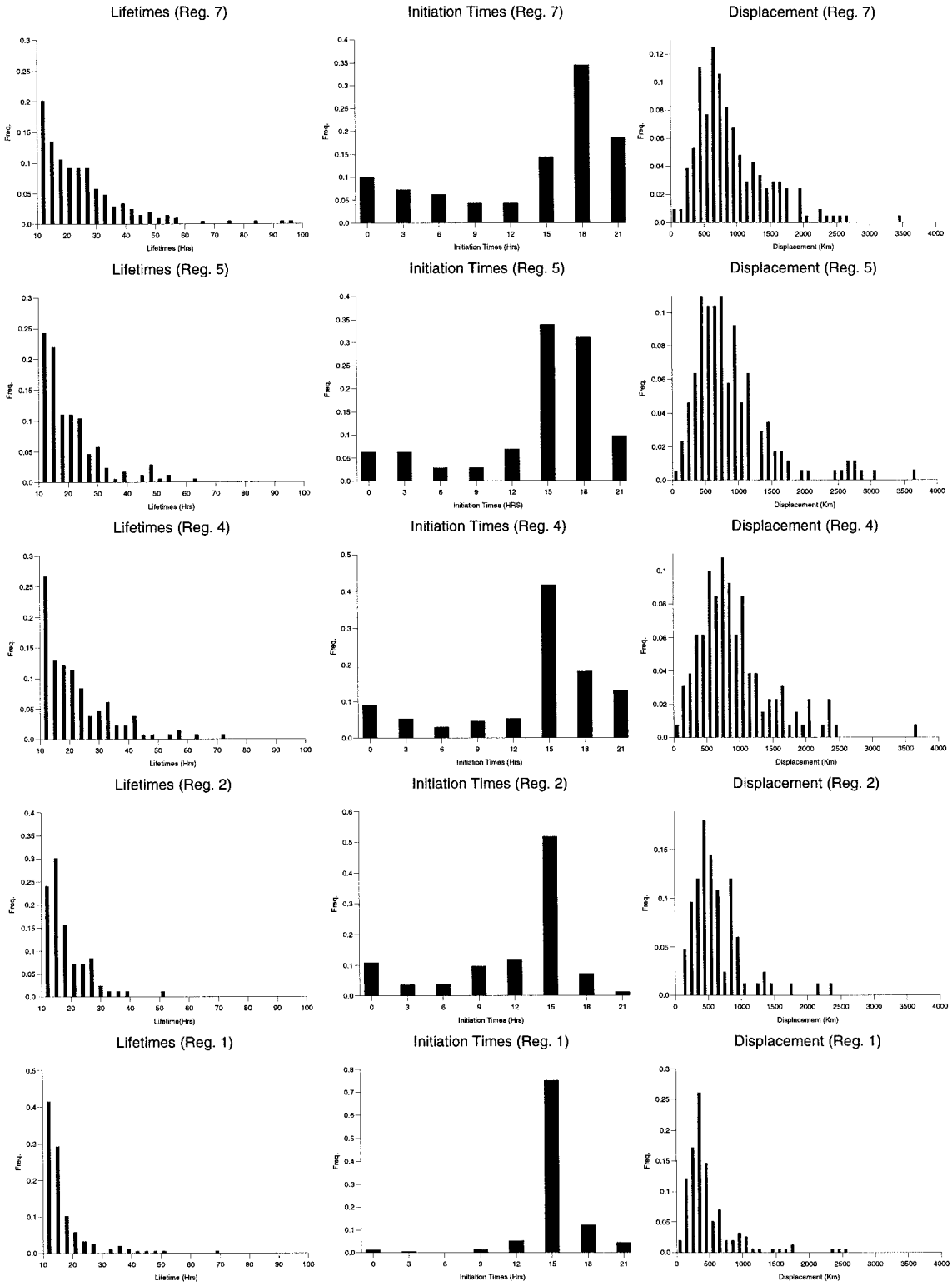

FIG. 10. Frequencies for lifetimes, initiation times, and displacements for systems that originate in the genesis regions.

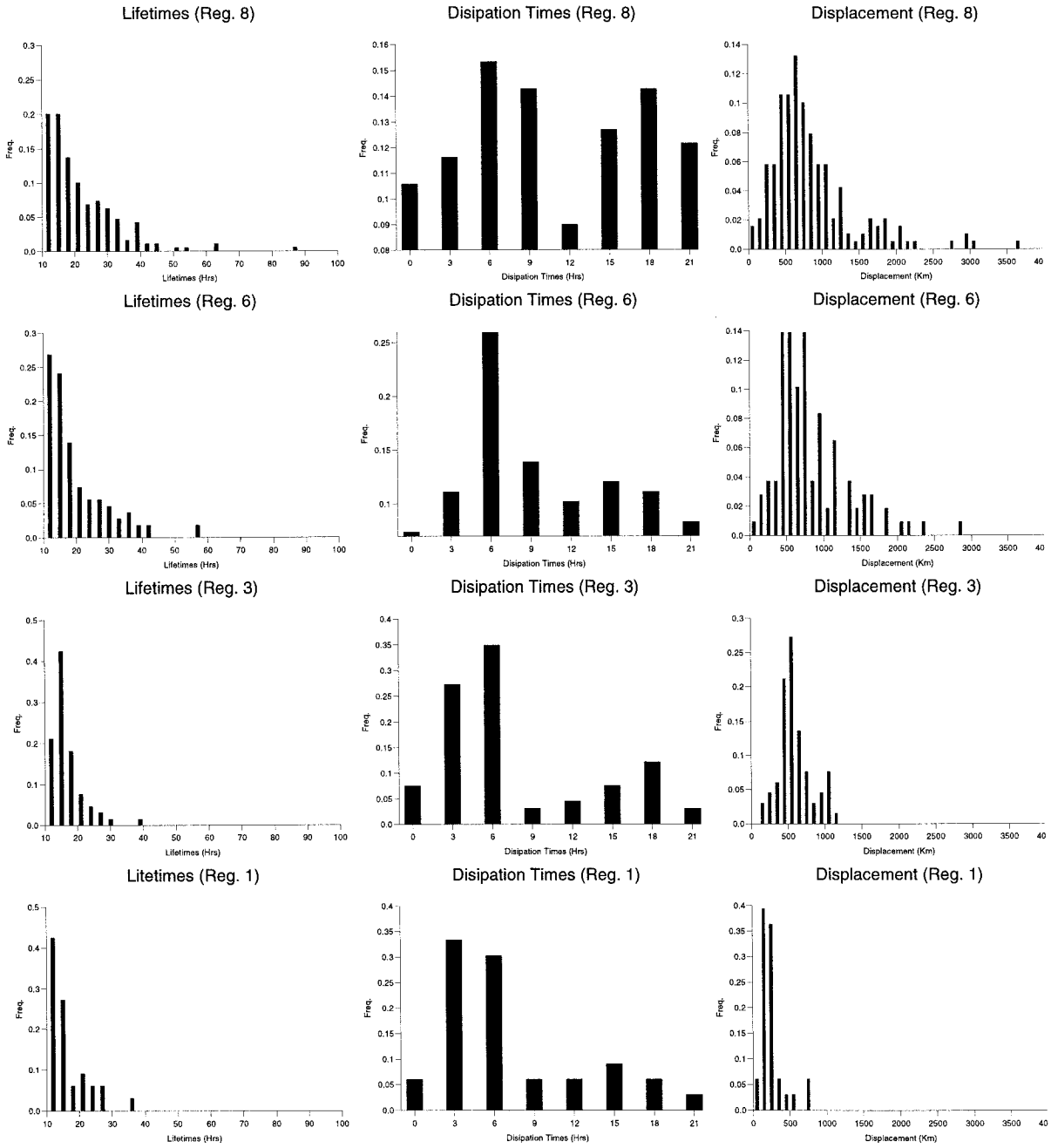

FIG. 11. Frequencies for lifetimes, dissipation times, and displacements for systems that dissipate within the lysis regions.

August and September. The lysis density maxima in July (Fig. 12a) is similarly shifted westward compared to the other months (cf. Figs. 1a,b, which show two squall lines that propagate into the ocean). In contrast, the genesis maximum over the Guinea highland coastal region is not shifted, remaining linked to the elevated terain. Thus, although throughout the season the ocean region downstream of the continent is not conducive to organized convective systems initiated over the land, for some reason these systems travel farther over the ocean in July. This occurs despite the fact that the SSTs are warmest in August in the convecting region. Examination of ECMWF reanalyses (not shown) shows very little difference in the low-level θ_e between July and August; it is in fact slightly higher in August, which is consistent with the higher SSTs.

It is well known that convection becomes disorganized as it moves from land to ocean (e.g., Carlson 1969). A better understanding of what determines whether the systems decay or manage to continue farther into the

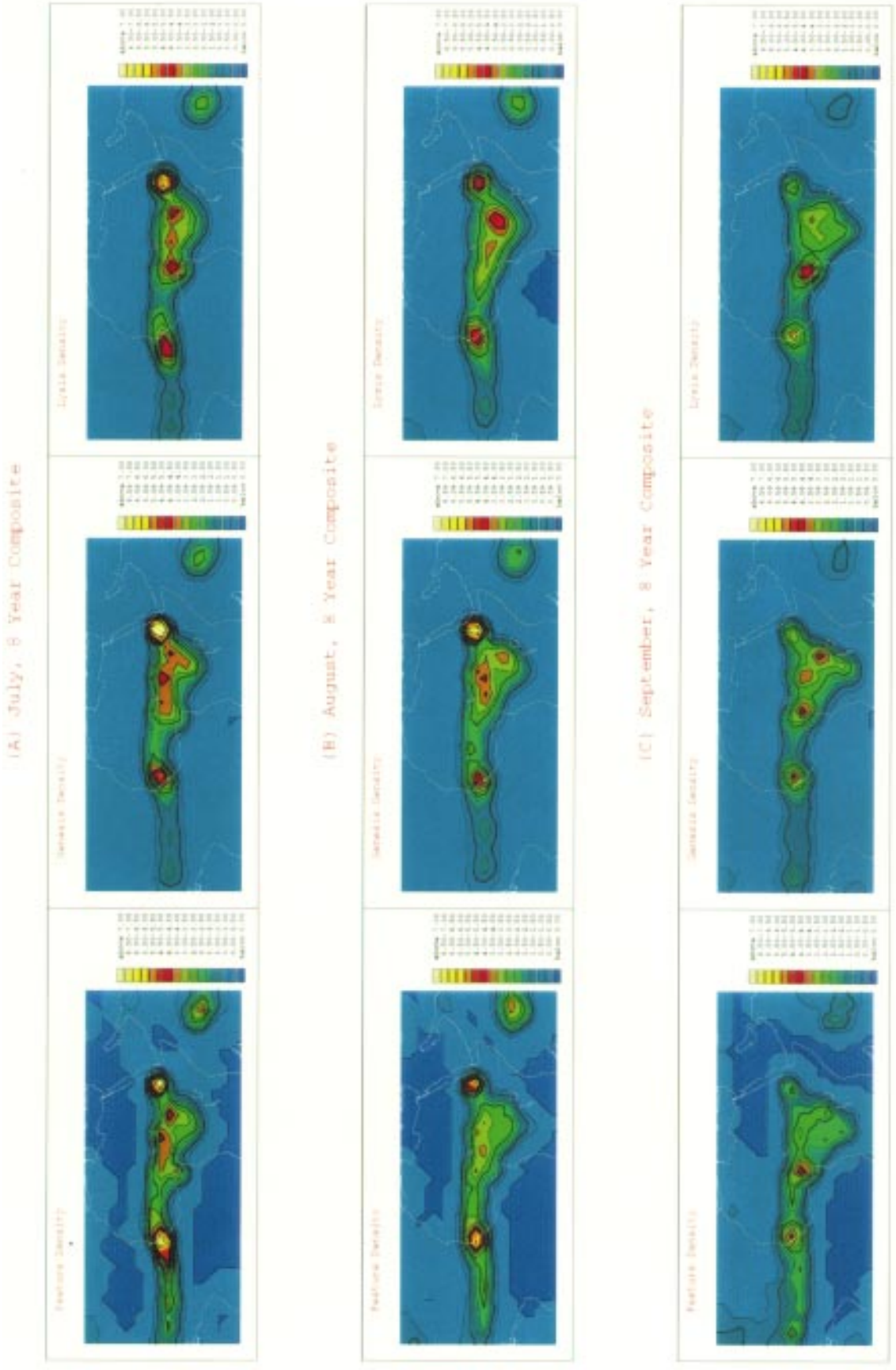

FIG. 12. Seasonal cycle (8-yr composite) statistics of feature density, genesis density, and lysis density for (a) July, (b) August, and (c) September.

central Atlantic may have some bearing on whether these systems play a role in tropical cyclogenesis.

5. Conclusions

This paper has shown how a long-term climatology of African convective complexes can be constructed from smoothed and gridded Meteosat data. The existing tracking algorithm has been modified to cope with missing images with some success. Climatological statistics have been produced that show the seasonal climatology with strong diurnal cycles over the land. Also seen is the shift to longer-lived systems and greater displacement distances in the west compared to the east within the main belt of activity. Much of this activity has been explained in terms of the thermodynamic and dynamic variables, confirming the importance of these quantities to the maintenance of organized convection. It has also been shown that the orography is important for both providing a trigger for convection and a barrier to propagating systems.

The results presented in this paper do not contradict any of the shorter timescale studies performed by previous authors (e.g., Desbois et al. 1988), but this longer timescale study provides a more representative description of the behavior of organized convection over tropical Africa and environs. It has been shown that the nature of the observed organized convection, such as the geographical distribution of initiation, dissipation, and the general motion are consistent with the ECMWF reanalyses and highlight the important role that vertical shear and potential and conditional instability play in the maintenence of organized convection for this region.

Future work in this area is directed toward more sophisticated means of feature detection on the technique side, and the analysis of the interannual variability of organized convection based on this approach of identification (using the improved techniques), tracking, and statistical analysis.

Acknowledgments. The data used for this study were obtained from the NASA Langley Research Center EOSDIS Distributed Active Archive Center.

REFERENCES

Arnaud. Y., M. Desbois, and J. Maizi, 1992: Automatic tracking and characterization of African convective systems on Meteosat pictures. *J. Appl. Meteor.,* **31,** 443–453.

Avila, L. A., and R. J. Pasch, 1992: Atlantic tropical systems of 1991. *Mon. Wea. Rev.,* **120,** 2688–2696.

Carlson, T. N., 1969: Some remarks on African disturbances and their progress over the tropical Atlantic. *Mon. Wea. Rev.,* **97,** 716–726.

Chong, M., P. Amayenc, G. Scialom, and J. Testud, 1987: A tropical squall line observed during the COPT 81 experiment in West Africa. Part I: Kinematic structure inferred from dual Doppler radar data. *Mon. Wea. Rev.,* **115,** 670–694.

Desbois, M., T. Kayiranga, B. Gnamien, S. Guessous, and L. Picon, 1988: Characterization of some elements of the Sahelian climate and their interannual variations for July 1983, 1984, and 1985 from the analysis of METEOSAT ISCCP data. *J. Climate,* **1,** 867–904.

Emanuel, K. A., 1994: *Atmospheric Convection.* Oxford University Press, 580 pp.

Hastenrath, S., 1991: *Climate Dynamics of the Tropics.* Kluwer Academic Publishers, 488 pp.

Hodges, K. I., 1994: A general method for tracking analysis and its application to meteorological data. *Mon. Wea. Rev.,* **122,** 2573–2586.

——, 1995: Feature tracking on the unit sphere. *Mon. Wea. Rev.,* **123,** 3458–3465.

——, 1996: Spherical nonparametric estimators applied to the UGAMP GCM integration for AMIP. *Mon. Wea. Rev.,* **124,** 2914–2932.

Laing, A. G., and J. M. Fritsch, 1993: Mesoscale convective complexes in Africa. *Mon. Wea. Rev.,* **121,** 2254–2263.

Landsea, C., and W. M. Gray, 1992: The strong association between western Sahel monsoon rainfall and intense Atlantic hurricanes. *J. Climate,* **5,** 435–453.

Machado, L. A. T., J. P. Duval, and M. Desbois, 1993: Diurnal variations and modulations by easterly waves of the size distribution of convective cloud clusters over West Africa and the Atlantic Ocean. *Mon. Wea. Rev.,* **121,** 37–49.

Maddox, R. A., 1980: Mesoscale convective complexes. *Bull. Amer. Meteor. Soc.,* **61,** 1374–1387.

Nicholson, S. E., 1980: The nature of rainfall fluctuations in subtropical West Africa. *Mon. Wea. Rev.,* **108,** 473–487.

Reed, R. J., D. C. Norquist, and E. E. Recher, 1980: Origin of African wave disturbances during Phase III of GATE. *Mon. Wea. Rev.,* **108,** 1827–1839.

Rossow, W. B., E. Kinsella, and A. Wolf, 1987: International Satellite Cloud Climatology Project (ISCCP) description of reduced resolution radiance data. World Meteorological Organization WMO/TD-No. 58, 143 pp.

Rowell, D. P., and J. R. Milford, 1993: On the generation of African squall lines. *J. Climate,* **6,** 1181–1193.

——, C. K. Folland, K. Maskell, and M. N. Ward, 1995: Variability of summer rainfall over tropical north Africa (1906–92): Observations and modelling. *Quart. J. Roy. Meteor. Soc.,* **121,** 669–704.

Thorncroft, C. D., and M. Haile, 1995: The mean dynamic and thermodynamic fields for July 1989 over tropical north Africa and their relationship to convective activity. *Mon. Wea. Rev.,* **123,** 3016–3031.

Weisman, M. L., and J. B. Klemp, 1982: The dependence of numerically simulated convective storms on vertical shear and bouyancy. *Mon. Wea. Rev.,* **110,** 504–520.

Williams, E., and N. Renno, 1993: An analysis of the conditional instability of the tropical atmosphere. *Mon. Wea. Rev.,* **121,** 21–36.